

Polymer Chemistry

Accepted Manuscript



This is an *Accepted Manuscript*, which has been through the Royal Society of Chemistry peer review process and has been accepted for publication.

Accepted Manuscripts are published online shortly after acceptance, before technical editing, formatting and proof reading. Using this free service, authors can make their results available to the community, in citable form, before we publish the edited article. We will replace this *Accepted Manuscript* with the edited and formatted *Advance Article* as soon as it is available.

You can find more information about *Accepted Manuscripts* in the [Information for Authors](#).

Please note that technical editing may introduce minor changes to the text and/or graphics, which may alter content. The journal's standard [Terms & Conditions](#) and the [Ethical guidelines](#) still apply. In no event shall the Royal Society of Chemistry be held responsible for any errors or omissions in this *Accepted Manuscript* or any consequences arising from the use of any information it contains.

ARTICLE

A facile route to diverse assemblies by host-guest recognition

Cite this: DOI: 10.1039/x0xx00000x

Xing Zhou^{a,b,†}, Songling Han^{a,‡}, Qixiong Zhang^a, Yin Dou^{a,b}, Jiawei Guo^a, Ling Che^{a,c}, Xiaohui Li^{*b}, Jianxiang Zhang^{*a}

Received 00th January 2012,

Accepted 00th January 2012

DOI: 10.1039/x0xx00000x

www.rsc.org/

Self-assembly provides a powerful approach for generating complex materials with advanced functionalities. Currently it remains a great challenge to create hierarchically structured assemblies from materials with simple molecular structure. Further, successful clinical translation of polymer assemblies-based therapeutics requires facile yet effective strategies for their fabrication and cargo loading based on structurally simple and cost-effective starting materials. Herein we partly addressed these issues by an all-in-one strategy involving host-guest assembly via molecular recognition, in which carboxyl-bearing compounds serve as guest molecules, while N-substituted acrylamide homopolymers or their various copolymers are host materials. Assembly and therapeutic loading can be simultaneously realized by this one-pot approach, leading to superstructures across length scales and with multiple morphologies, such as micelle-like nanoparticles, vesicles, nano- and microspheres, microtubes, and onion-like multilayer structures. In addition to biomedical applications, superstructures generated by this simple and robust strategy have potential uses in templated synthesis, catalysis, optics, and microelectronics.

Introduction

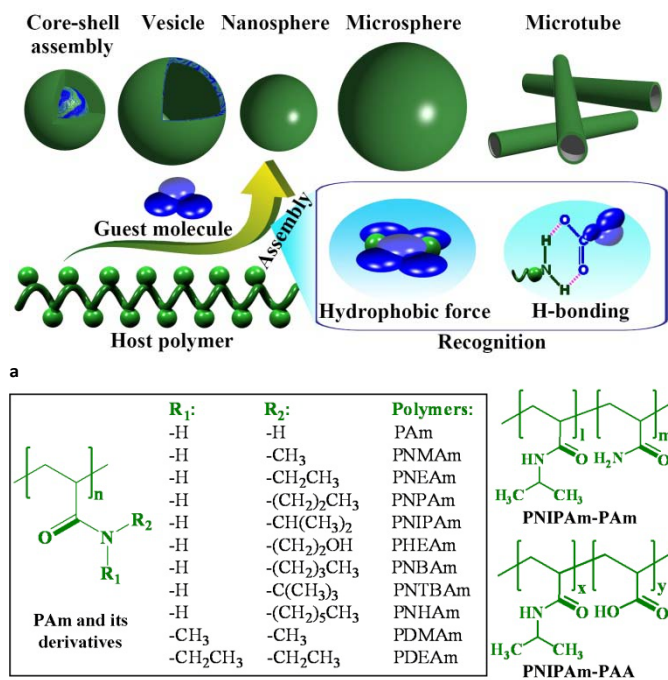
Self-assembly of complex materials with advanced functionalities has received considerable attention in many areas of materials science and engineering.¹⁻⁸ These artificial superstructures, across all length scales, have broad applications varying from catalysis,⁹ optics,¹⁰ microelectronics,¹¹ nanolithography,¹² biotechnology,¹³ biosensing,¹⁴ tissue regeneration,¹⁵ to drug delivery¹⁶ and gene therapy.¹⁷ To realize these functional materials via self-assembly, numerous molecular building blocks with diverse chemical structures have been utilized, including lipids,¹⁸ surfactants,¹⁹ peptides,²⁰ proteins,²¹ DNAs,²² RNAs,²³ and polymeric amphiphiles² as well as molecular hosts with converged binding sites and guest molecules.²⁴⁻²⁶ Intensive studies on self-assembly of polymers bearing two or more chemically different components have successfully produced enormous superstructures like multimorphological micelles (spherical,²⁷ wormlike,²⁸ multicompart, and cylindrical³⁰), polymersomes,³¹ toroidal assemblies,³² striped cylinders³³ as well as macroscopic tubes.^{34, 35} These hierarchically structured assemblies with different dimensions were largely created from architecturally complex polymers with linear, cyclic, star, graft, dendron, or hyperbranched topologies. Manipulation on scale and morphology of polymer assemblies generally requires

elegant molecular design, sophisticated synthesis, and delicate processing control. It remains a great scientific and engineering challenge to craft assemblies with controlled size, shape, composition, and internal structure as well as customized functionalities.

On the other hand, successful bench-to-bedside translation of a plethora of therapeutics derived from polymer assembly has been hampered by difficulties in the large-scale synthesis of topological copolymers with tailored structures, such as good quality control and reproducible manufacturing.³⁶ In some cases, the poor drug loading capability and relatively high production cost of therapeutic polymer assemblies are additional issues limiting their clinical translation.³⁷ Consequently, there is still unmet demand for discovering facile and cost-effective assembly strategies to create different superstructures with good scalability and repeatability.³⁸ Simply mixing two or more complementary molecular constituents represents an intriguing approach towards superstructured functional materials. Nevertheless, building components currently discovered exhibit significant limitations with respect to size tailoring, structure modulation, assembly efficiency and yield, as well as desirable biomedical performances. Herein we describe a simple and robust method for structuring diverse and functional polymeric superstructures by a one-step route based on guest molecules-

directed assembly of structurally simple materials via molecular recognition.

Results and discussion

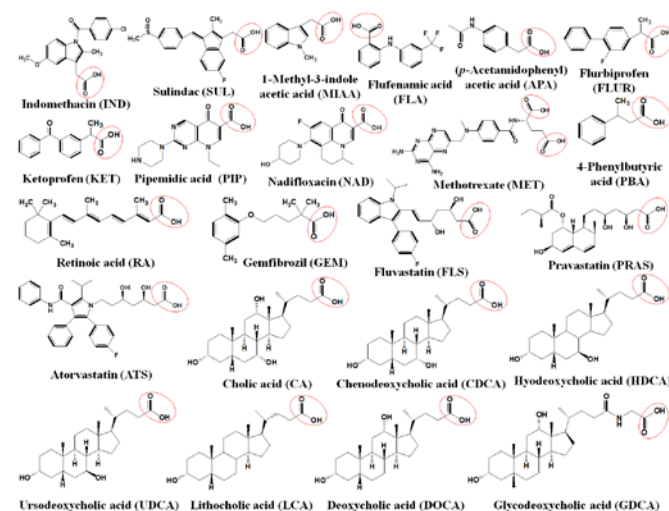


Scheme 1 Self-assembly of multiple morphological superstructures across length scales by carboxyl-bearing compounds (CBCs) and structurally simple starting materials. **a**, Schematic showing the formation of diverse assemblies by poly(*N*-isopropylacrylamide) (PNIPAm) and CBCs via molecular recognition. **b**, Chemical structures of polyacrylamide (PAm) and its derivatives involved in this study.

Host molecules-mediated assembly of poly(*N*-alkylacrylamide)s

We speculate that formation of superstructures and therapeutics packaging can be simultaneously achieved by cargo molecules-directed assembly of host polymers, given that there are multiple synergistic forces between the guest and the host (Scheme 1a). By varying the content of guest molecules, the hydrophilic-hydrophobic balance of the host-guest system may be regulated, thereby modulating the scale and shape of resulting assemblies. As a proof of concept, initially we selected polyacrylamide (PAm) and its two derivatives of poly(*N*, *N*-dimethylacrylamide) (PDMAm) and poly(*N*-isopropylacrylamide) (PNIPAm, Scheme 1b and Table S1) as starting materials with simple chemical structure. All of them are water-soluble polymers with polar amide and hydrophobic units. This structural feature affords potential hydrogen bonding (H-bonding) and hydrophobic interactions with other molecules. With this in mind, we started our studies by screening a library of structurally diverse hydrophobic carboxyl-bearing compounds (CBCs). PAm, PDMAm, and PNIPAm may interact with these CBCs through both H-bonding and hydrophobic interactions, since their amide is able to interact with carboxyl via H-bonding,³⁹ while hydrophobic forces exist

between their lipophilic moieties. Firstly, common aliphatic acids including valeric acid (VAL), hexanoic acid (HEX), and heptanoic acid (HEP) were used as model compounds. The assembly was conducted by directly mixing polymers and organic acids in aqueous solution. To intuitively show assemblies, trace amount of Nile red was dissolved in the organic acid for fluorescence labeling. Observation by confocal laser scanning microscopy (CLSM) revealed well-dispersed spherical particles formed by the mentioned various polymer-acid pairs (Fig. S1a-c), and their size was dominated by the materials structure and their ratios (Fig. S1d). The formation of disseminated spherical assemblies was verified by transmission electron microscopy (TEM, Fig. S1e). Measurement by isothermal titration calorimetry (ITC) suggested thermodynamically favorable binding between these amide-containing polymers and aliphatic acids (Fig. S1f-g). These preliminary results demonstrated the feasibility of constructing discrete assemblies by CBCs-mediated assembly of hydrophilic PAm and its derivatives.



Scheme 2 Chemical structures of typical biologically active CBCs.

On the basis of these findings, we examined a series of CBCs with biological or pharmacological activities (Scheme 2 and Table S2), with the aim to achieve therapeutic loading concomitant with assembly, which is more significant for engineering assemblies for drug delivery. We first employed indomethacin (IND), a nonsteroidal anti-inflammatory drug (NSAID) clinically used for the treatment of osteoarthritis, rheumatoid arthritis, and ankylosing spondylitis. PAm and its derivatives with different *N*-substituted groups were screened to interrogate structural effects of the host polymers, including PAm, PDMAm, PNIPAm, poly(*N*-methylacrylamide) (PNMAm), poly(*N*-ethylacrylamide) (PNEAm), poly(*N*-propylacrylamide) (PNPAm), poly(*N*-hydroxyethylacrylamide) (PHEAm), poly(*N*-butylacrylamide) (PNBAm), poly(*N*-*tert*-butylacrylamide) (PNTBAm), poly(*N*-hexylacrylamide) (PNHAm), and poly(*N*, *N*-diethylacrylamide) (PDEAm) (Scheme 1b and Table S1). Among them, PAm has the strongest H-bonding with carboxyl, because almost no steric

hindrance exists in this case, while polymers with more hydrophobic substitution may have stronger hydrophobic interactions with lipophilic CBCs. The dialysis procedure was implemented for assembly according to the solubility characteristics of the involved polymers and IND, with dimethyl sulfoxide (DMSO) as a common solvent. Dialysis of IND/PAm at a weight ratio 1:1 in DMSO against water led to drug crystals as illustrated by scanning electron microscopy (SEM, Fig. 1a). Introducing another polar group in the mono-N-substitution of the host polymer that may enhance H-bonding did not positively contribute to the guest-mediated assembly, as evidenced by PHEAm. For PDMAm and PDEAm that have impaired H-bonding but stronger hydrophobic forces with IND in comparison to PAm, we also observed drug crystals other than structured assemblies. As for mono-N-substituted polymers (such as PNMAm, PNEAm, PNBAm, PNTBAm, and PNHAM), with both H-bonding and hydrophobic interactions with IND, dialysis of drug/polymer mixture at 1:1 gave rise to IND crystals concomitant with some spherical particles. By contrast, well-defined spherical assemblies with mean size of 712 and 630 nm were produced for PNPAm and PNIPAm at the IND/polymer weight ratio of 1:1, respectively. To realize the host-mediated guest assembly, CBC-polymer interactions must be strong enough to conquer noncovalent forces among CBC molecules, thereby preventing crystallization of the hydrophobic guest molecules. For IND, a repertoire of H-bonding, *van der Waals*, π - π stacking, and hydrophobic interactions account for molecular packing and subsequent crystallization. As for PAm and PHEAm, H-bonding dominates the drug-polymer interaction, while hydrophobic forces govern in the case of PDMAm and PDEAm as well as PNBAm, PNTBAm, and PNHAM.

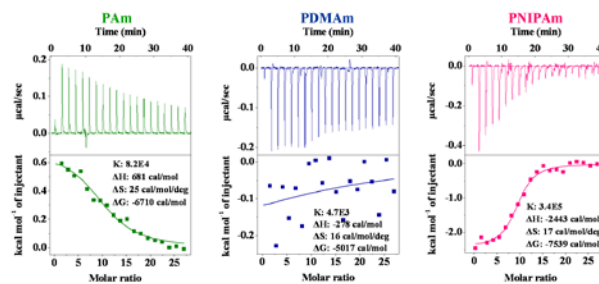
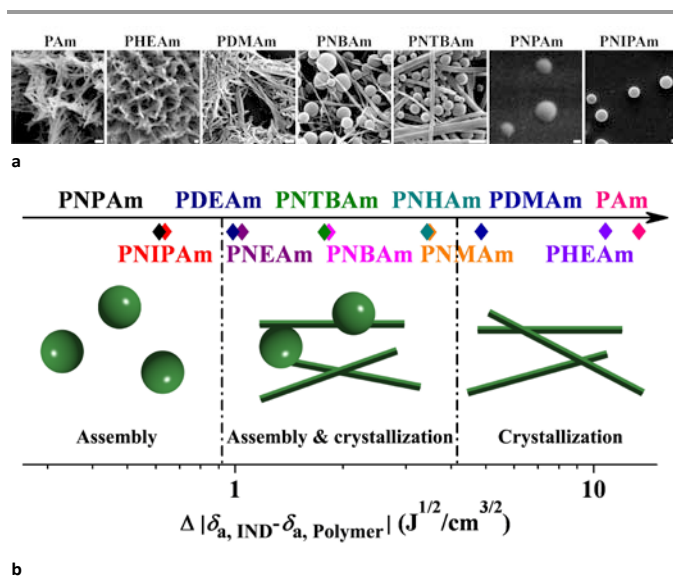


Fig. 1 Effects of structure of homopolymers on assembly. **a**, SEM images showing assemblies, polymer/IND aggregates, or IND crystals. **b**, Molecular structures of polymers dominating their assembly with IND molecules. The graph and in-set cartoons indicating the effect of δ_a differences between polymer and IND on assembly behaviors of various combinations. Scale bars, 500 nm. **c**, ITC curves and fitting plots of IND/PAm, IND/PDMAm, and IND/PNIPAm.

In order to form assemblies, the collective effect of H-bonding and hydrophobic interactions between a CBC and a host polymer should surmount that among CBC molecules, and consequently assembly of this host-guest system necessitates their synergistic action. Together, these results suggested that selective recognition between a CBC and a host polymer that may maximize their interactions is imperative for successful assembly. As for the discrepancy between IND and liquid aliphatic acids (such as VAL, HEX, and HEP that can assemble with PAm, PDMAm, and PNIPAm to form spherical assemblies), it might be largely attributed to the difference in cohesive energy (CE) as well as the presence or absence of the common solvent. The calculated values of both CE and cohesive energy density (CED) of these aliphatic acids are notably lower than those of IND (Table S3).

Characterization of host-guest interactions

With the attempt to understand mechanisms underlying this host-guest assembly, we calculated solubility parameters (δ) of various polymers and IND, as the differences in δ values have been frequently used to predict compatibility between polymers and small molecules.⁴⁰ According to the theory developed by Hildebrand, $\Delta H = \varphi_1 \varphi_2 (\delta_1 - \delta_2)^2$ (where φ_1 and φ_2 denote the volume fraction of two components), the maximal compatibility will be achieved when δ_1 approaches δ_2 . Both partial and total δ were calculated by a group contribution method as described previously.⁴¹ Whereas the differences in total δ values did not predict the observed guest-host assembly behaviors, δ_a , defined as polar δ , showed good prediction (Fig. 1b). For IND/polymer mixtures (such as PAm, PHEAm, and PDMAm) with larger δ_a differences, drug molecules tended to crystallize to macroscaled aggregates composed of nanofibrous crystals. By contrast, the IND/PNPAm and IND/PNIPAm pairs gave the smallest difference in δ_a values, which is in good agreement with their assembly performance. Other combinations with moderate differences afforded both spherical assemblies and drug crystals. In this context, only a limited number of drug molecules might participate in assembly, while excessive IND molecules may crystallize. Since δ_a is derived from partial δ of δ_p and δ_h ($\delta_a = (\delta_p^2 + \delta_h^2)^{1/2}$) that are contributed by dipole-dipole interactions and H-bonding,⁴² respectively; δ_a is closely related to

association interactions. According to Bagley et al.,⁴³ $CEd - P_i = \delta_p^2 + \delta_n^2 = \delta_a^2$ (where P_i is the internal pressure), while $CEd - P_i$ measures the intermolecular binding energy; consequently assembly of IND/host polymers is strongly dominated by polar interactions and H-bonding. These forces are reciprocally associated with the volume of hydrophobic moieties, as a big hydrophobic group causes steric effect and prevents close association of polar groups.

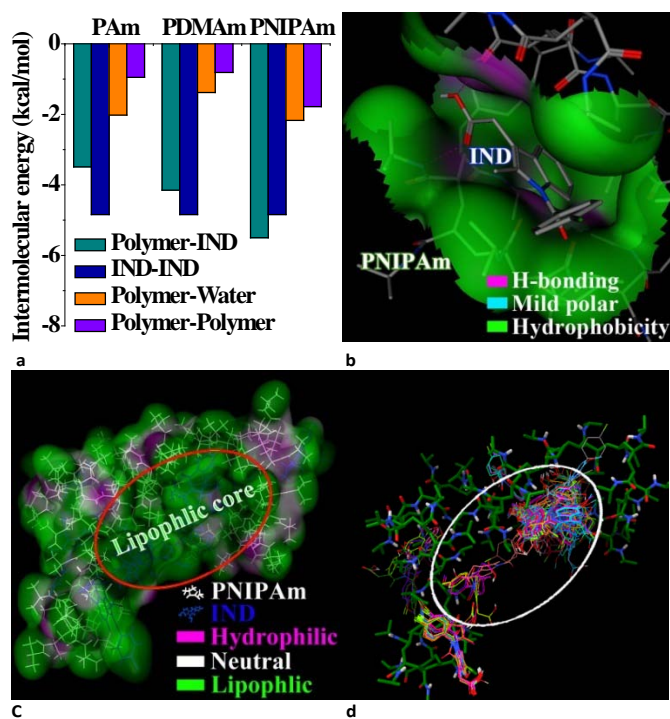


Fig. 2 Computational simulation of drug-polymer interactions. **a**, The calculated intermolecular energy of various components in IND/polymer mixture. **b**, The lowest energy 3D conformation of IND docked into PNIPAm. **c**, The 3D style showing distribution of various molecules at the IND/PNIPAm molar ratio of 10/1 after 5 ns of MD process. The carbon, oxygen, nitrogen, and polar hydrogen (that can form H-bonding) atoms are indicated by gray, red, dark blue, and light gray, respectively. The surface interaction sites and lipophilicity were drawn and colored by the Connolly method. **d**, The main putative sites for IND molecules docked in a PNIPAm chain that was optimized by MD modeling of IND/PNIPAm at the molar ratio of 10/1.

We further characterized guest-host pairs based on typical water-soluble polymers of PAm, PDMAm, and PNIPAm by ITC. Positive ΔH was measured for IND/PAm (Fig. 1c), indicating an endothermal process. For PDMAm, however, the titration data even could not give a good fitting, implying that almost no binding occurred in this case. On the other hand, negative enthalpy of the IND/PNIPAm system revealed an exothermal profile. Besides, the biggest negative ΔG value was calculated for IND/PNIPAm. These results demonstrated that, although detectable binding occurred for both PAm and PNIPAm, assembly of IND/PNIPAm is thermodynamically favored. To validate this point, computational modeling was conducted to simulate guest-host interactions. The AutoDock program was used to estimate the docking energy and intermolecular energy of the assembly system containing water, IND, and a representative polymer of PAm, PDMAm, or

PNIPAm. Since binding sites in the polymer were not defined, the blind docking was applied to the entire polymer chain and the drug molecule. In IND/PAm and IND/PDMAm, the biggest intermolecular energy was observed for IND-IND, followed by IND-polymer, polymer-water, and polymer-polymer (Fig. 2a). In IND/PNIPAm, however, the intermolecular energy of IND-PNIPAm was highest among all combinations. This suggested that IND-PNIPAm interaction can overcome other forces that impede assembly. On the contrary, IND-PAm or IND-PDMAm interaction cannot surmount IND-IND forces, and accordingly drug molecules are prone to crystallization. This well agrees with our experimental results (Fig. 1a). After the docking calculation, the lowest energy conformation of IND within the PNIPAm chain exhibited a big pocket formed by the side groups and backbone of PNIPAm, and IND was exactly “embraced” by the carbochain via hydrophobic areas and by carbonyl via H-bonding (Fig. 2b). Estimation of the contribution of different forces to the total free energy of IND-PNIPAm binding revealed that the majority was offered by H-bonding and *van der Waals* interactions (Fig. S2a), while electrostatic interaction is of marginal importance. Subsequently, this IND/PNIPAm complex was employed to perform molecular dynamic (MD) simulation. Two new H-bonding sites were formed between IND and PNIPAm nearly in the whole MD process (Fig. S2b-c), and both hydrophobic and H-bonding energy as well as the total binding energy was significantly enhanced (Fig. S2d). This indicated that, in comparison to the initial docking state, IND-PNIPAm interactions increased during their assembly process by regulating PNIPAm to a more comfortable conformation. Additionally, MD modeling of IND/PNIPAm at a molar ratio of 10/1 was performed to simulate the assembly process at a high IND feeding. After 5 ns of dynamic process, IND/PNIPAm entangled chains into a nearly spherical shape with eight IND molecules caught by the PNIPAm pocket containing both hydrophobic and H-bonding areas (Fig. 2c), and a big hydrophobic area formed in the assembly core which was mainly composed of the PNIPAm backbone and IND molecules. Besides, the PNIPAm conformation thus obtained was maintained to conduct docking with IND to find the putative binding sites (like those of proteins) in IND/PNIPAm. Similar to the MD simulation results, we found that almost 80% of docking runs were accumulated in the core of IND/PNIPAm assembly (Fig. 2d). This is coincident with the hydrophobic core consisted of the PNIPAm backbone and IND molecules in the MD simulation. These results implied that multiple non-covalent interactions contribute to IND/PNIPAm assembly from a computational point of view, which include H-bonding, *van der Waals*, hydrophobic, and electrostatic interactions.

We then experimentally characterized non-covalent forces dominating IND/PNIPAm assembly by Fourier transform infrared (FT-IR) and NMR spectroscopy. The antisymmetric stretching vibration at 1712 cm^{-1} due to IND carbonyl gradually weakened as the PNIPAm content was increased (Fig. S3a). In addition, the amide bond I due to carbonyl in PNIPAm at 1654 cm^{-1} was shifted to 1689 cm^{-1} as the IND content enhanced.

These changes in absorption of carbonyl from both IND and PNIPAm implied the presence of H-bonding between them. Symmetric deformation vibration bonds of isopropyl in PNIPAm (at 1368 and 1388 cm^{-1}) were attenuated with increasing IND (Fig. S3b). Furthermore, the bond at 1388 cm^{-1} was more significantly impaired compared with that at 1368 cm^{-1} (Fig. S3c). This may suggest that the microenvironment of isopropyl was changed after assembly with PNIPAm, indicating the existence of hydrophobic interactions between isopropyl and lipophilic moieties of IND. IND-PNIPAm interactions were also verified by the ^1H - ^1H Noesy NMR spectrum, from which correlation between proton signals at 1.0 and 7.0-7.6 ppm was observed for IND/PNIPAm mixture in DMSO-d_6 (Fig. S4), implicating interactions between isopropyl and aryl groups. Collectively, these studies corroborated that there are both H-bonding and hydrophobic interactions between IND and PNIPAm. Consistent with these findings, assembly did not happen when H-bonding of IND-PNIPAm was destroyed by elevating temperature to 50°C (Fig. S5). In aqueous solution, PNIPAm has a lower critical solution temperature (LCST) at 32°C. At higher temperatures, hydrophobic forces of polymer chains are strengthened, while H-bonding of IND-PNIPAm may be remarkably attenuated due to breakage by temperature agitation.⁴⁴ Also, presence of competitive compounds that are able to form H-bonding with IND or PNIPAm impeded IND/PNIPAm assembly. For example, addition of either thiourea (a strong competitor of PNIPAm) or acetic/propionic acid (competitive molecules of IND) during assembly resulted in drug crystals (Fig. S6). It is worth noting that the carboxyl proton of IND might transfer to the amide group of PNIPAm by undergoing an acid-base reaction. This may lead to electrostatic interactions between IND and PNIPAm, which should also account for the observed host-guest assembly.

Assemblies formed by PNIPAm and IND

As a water-soluble thermosensitive polymer, PNIPAm has been frequently used as a component to construct various temperature responsive systems, such as molecular conjugates, nano- and microparticles, and hydrogels.⁴⁵ Consequently, PNIPAm-based systems were intensively examined. For supramolecular assemblies derived from amphiphilic molecules, their morphology is strongly related to the hydrophilic-hydrophobic balance of materials.^{28, 31, 46} We therefore investigated the CBC content-dependent structural evolution of IND/PNIPAm assemblies. At IND/PNIPAm feeding ratios of 0.1:1, 0.2:1, and 0.3:1 (the actual IND loading was 9.0%, 16.5%, and 22.5%, respectively), nanoassemblies with average diameter of 80, 159, and 246 nm were achieved, respectively (Fig. 3a and S7a). Evident core-shell structure could be observed for assemblies at 0.2:1 and 0.3:1. When IND feeding increased to 0.5:1, 0.7:1, and 1:1 (the resultant IND content was 32.6%, 41.0%, and 50.1%, respectively), vesicles were formed as clearly imaged by TEM (the average size was 439, 549, and 628 nm, respectively). The vesicular structure was also confirmed by CLSM, taking advantage of the intrinsic fluorescence of IND (Fig. 3a). Further increasing IND (at 2:1,

2.5:1, and 3:1, and the corresponding IND content was 60.6%, 66.5%, and 74.5%, respectively) led to either solid nanospheres or microspheres, with size varying from 746 to 1042 nm (Fig. S7a). Accordingly, morphology of IND/PNIPAm assemblies can be manipulated by varying the content of guest molecules. This hydrophobic content governed morphological evolution is similar to that observed for superstructures assembled by amphiphilic molecules.^{28, 31} Whereas the exact mechanism remains elusive and warrants additional investigation, growth of these assemblies is considered to be related with the formation of pseudo-amphiphiles from PNIPAm/IND via non-covalent bonding. At low contents of IND, only a small number of IND molecules bind with PNIPAm to form pseudo-amphiphilic chains with relatively low hydrophobicity, finally resulting in micelle-like core-shell particles (the lower panel of Fig. 3a). Further increasing the IND content hydrophobizes the amphiphilic polymer/IND pairs, and to a certain degree morphological transition from core-shell to vesicular structure may occur. Additionally enhanced IND feeding generates solid nanospheres, probably resulting from IND-enriched PNIPAm/IND pairs with predominant hydrophobicity. It should be emphasized that in all cases, besides bound IND molecules, free ones may be incorporated due to hydrophobic interactions.

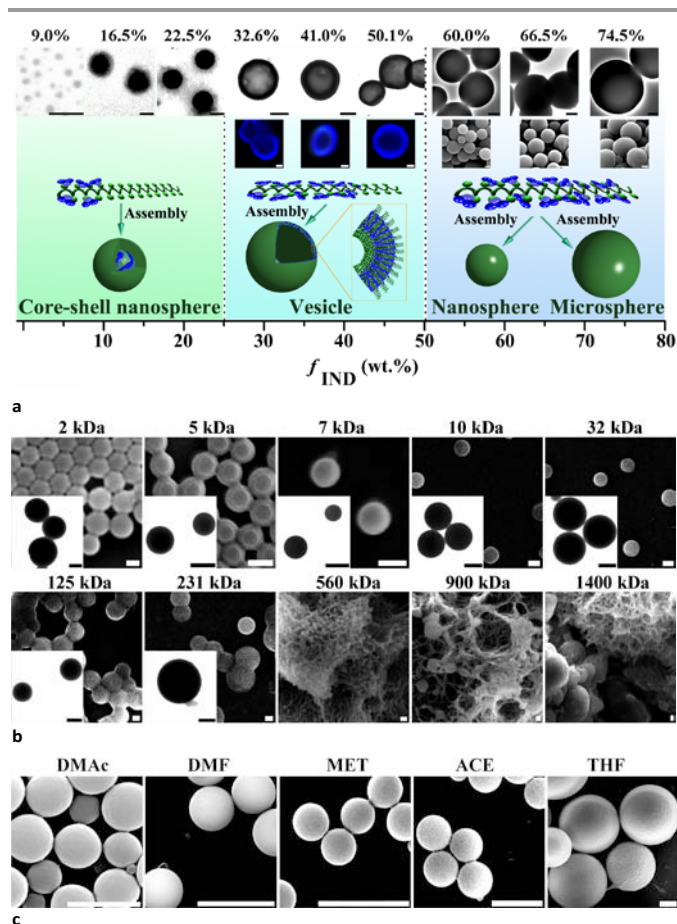


Fig. 3 The influence of different parameters on assembly. **a**, The drug content dependent morphological evolution of IND/PNIPAm assemblies. The upper panel shows TEM, CLSM, and SEM images of assemblies with various drug contents. The lower panel reveals correlation between IND contents and assembly

structures originated from PNIPAm with Mw of 7 kDa. For images at 9.0%, 16.5%, and 22.5%, the scale bar is 100 nm, while others represent 500 nm. **b**, SEM images of IND/PNIPAm assemblies or aggregates derived from PNIPAm with different molecular weights. The inset images showing corresponding TEM images. Scale bars, 500 nm. **c**, SEM images of IND/PNIPAm microspheres assembled using various processing solvents. The weight ratio of IND/PNIPAm was 1.5:1. Scale bars, 2 μ m.

Further, we examined factors dominating IND/PNIPAm assembly, including the molecular weight (Mw) of PNIPAm, PNIPAm configuration, and the type of common solvents. At the constant IND/PNIPAm ratio of 2:1, well-defined spherical assemblies with average size of 633 ± 108 , 581 ± 48 , 611 ± 99 , 688 ± 95 , 708 ± 92 , 1031 ± 109 , and 1706 ± 279 nm were obtained as PNIPAm with Mw of 2, 5, 7, 10, 32, 125, and 231 kDa was used, respectively (Fig. 3b and S7b). At high Mw of 560, 900, and 1400 kDa, however, IND crystallized to large aggregates, and only a few spherical particles could be observed. This revealed that PNIPAm with extremely high Mw cannot fully co-assemble with IND. According to previous studies, single chains of high Mw PNIPAm may undergo coil-to-globule transition in water, resulting in thermodynamically stable collapsed globules.⁴⁷ Compared with the expanded coil, the collapsed conformation exposes less amide units, which is detrimental to effective interactions between amide and IND. Also, we found that the polymer configuration has a profound effect on IND/PNIPAm assembly. When isotactic PNIPAm (isoPNIPAm) was explored, no assemblies could be obtained at various IND/isoPNIPAm feedings (Fig. S8). As isoPNIPAm is more rigid than atactic PNIPAm, polymer chains with high rigidity and less flexibility may not benefit host-guest interactions. Consequently, IND/PNIPAm assembly is selective to polymer stereoregularity, and only atactic PNIPAm is favorable to assembly. For polymer assemblies fabricated through solution-based processes, their size and shape can be tailored by solution conditions.⁴⁶ Likewise, assembly of IND/PNIPAm depended on common solvents. At IND/PNIPAm feeding of 1.5:1, their co-assembly gave rise to narrowly dispersed nano- or microspheres of varied size when dimethylacetamide (DMAc), dimethylformamide (DMF), methanol (MET), acetone (ACE), or tetrahydrofuran (THF) was separately used (Fig. 3c and S7c). Particularly, microspheres with mean size of 6.3 μ m were achieved when THF was utilized. These results revealed that the scale of these spherical assemblies can be partly tuned from hundreds of nanometers to tens of micrometers simply by changing the solvent. Interestingly, size of these assemblies was intimately related to the dielectric constant (ϵ) of employed solvents (Fig. S7c). Solvents with high ϵ generally yielded smaller particles, while low ϵ solvents generated bigger ones.

Structural effects of CBCs and host polymers on assembly

| MIAA | SUL | FLUR |
|------|-----|------|
|------|-----|------|

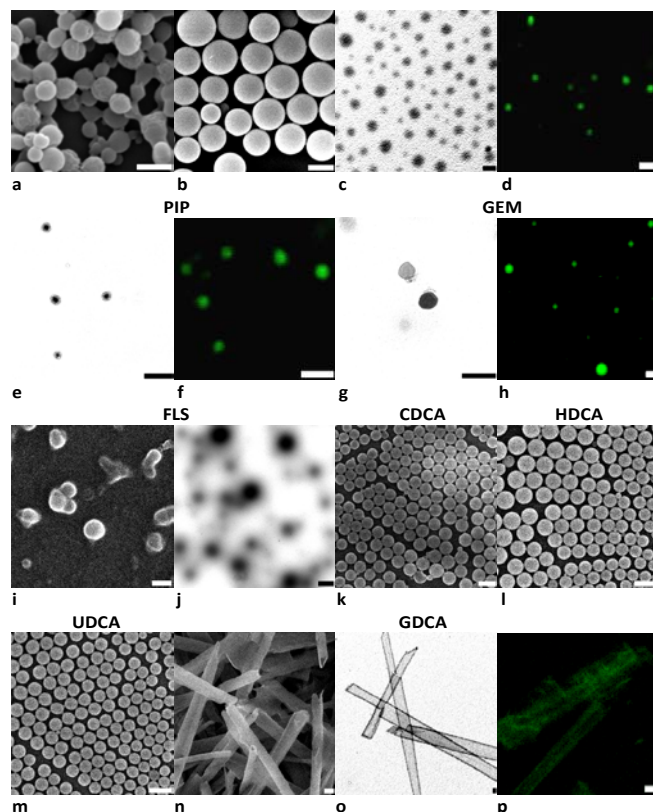


Fig. 4 Diverse superstructures formed by different pharmacologically active CBCs and PNIPAm. **a-p**, SEM, TEM, and CLSM images of assemblies from PNIPAm and various CBCs. For GDCA, the weight ratio of CBC/PNIPAm was 3:1, while it was 2:1 in other cases. The scale bar represents 200 nm for TEM images, while it is 1 μ m for SEM and CLSM images.

Next, we investigated structural dependence of this host-guest assembly. Various pharmacologically active CBCs were used (Scheme 2), including other NSAIDs, antibacterial drugs, antitumor drugs, drugs for cardiovascular disease, and reagents for biliary diseases (Table S2). As illustrated by microscopy imaging, anti-inflammatory drugs such as sulindac (SUL), 1-methyl-3-indoleacetic acid (MIAA), flufenamic acid (FLA), *p*-acetamidophenyl acetic acid (APA), flurbiprofen (FLUR), and ketoprofen (KET), all could mediate PNIPAm assembly to form spherical particles of various sizes at a drug/polymer ratio of 2:1 (Fig. 4a-c, S9a-c, and S10a). Spherical assemblies were also obtained when antibacterial agents of pipemidic acid (PIP) and nadifloxacin (NAD) as well as an antimetabolite drug of methotrexate (MET) were utilized (Fig. 4e and S9d-e). Drugs for prevention and treatment of cardiovascular disease, including 4-phenylbutyric acid (PBA), retinoic acid (RA), gemfibrozil (GEM), fluvastatin (FLS), pravastatin (PRAS), and atorvastatin (ATS) could also serve as guest molecules to initiate assembly, producing sphere-shaped nanoassemblies (Fig. 4g, 4i, and 4j, Fig. S9f-i and S10a). Fluorescence imaging using fluorescein-labeled PNIPAm (Mw = 25 kDa) further confirmed formation of spherical assemblies in the case of FLUR, PIP, and GEM (Fig. 4d, 4f, and 4h). Also, we found spherical assemblies as CBCs were cholic acid (CA) and its derivatives like chenodeoxycholic acid (CDCA),

hydoxycholeic acid (HDCA), ursodeoxycholeic acid (UDCA), lithocholic acid (LCA), and deoxycholeic acid (DOCA) (Fig. 4k-m, S9j-l, and S10a). Of note, narrowly dispersed nanospheres were produced when CDCA, HDCA, and UDCA were used. Interestingly, whereas 0.85 μm -microspheres were formed by glycodeoxycholeic acid (GDCA)/PNIPAm at 0.5:1 (Fig. S9m), increasing their ratio to 3:1 resulted in microtubes as indicated by cross-section structure in the SEM image (Fig. 4n). This microtubular structure, with average length of $\sim 20 \mu\text{m}$ and mean diameter of about 1.5 μm , was further affirmed by TEM and fluorescence microscopy using fluorescein-labeled PNIPAm (Fig. 4o-p). The formation of this tubular structure might be attributed to helical stacking of GDCA molecules that noncovalently associate with PNIPAm chains,⁴⁸ leading to stable exterior and interior surfaces covered by hydrophilic PNIPAm segments without binding with guest molecules. Nevertheless, additional studies are necessary to support this hypothesis. Accordingly, these results manifested multi-morphological assemblies across multiple length scales can be constructed by host-guest assembly of PNIPAm and various bioactive CBCs, with their features depending on the structure and content of hydrophobic guest molecules.

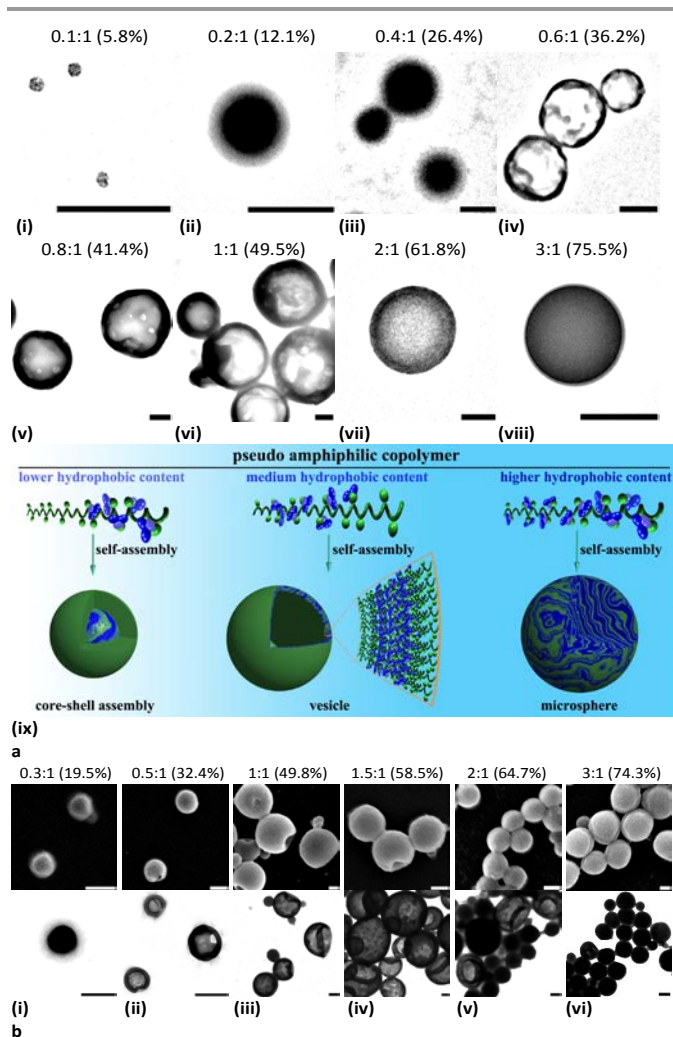


Fig. 5 Multiple-structured assemblies afforded by IND and PNIPAm copolymers. **a**, TEM micrographs illustrating assemblies originated from a random copolymer of PNIPAm-PAA at different contents of IND. **b**, SEM and TEM images of assemblies based on IND and a block copolymer of PNIPAm-PAA at various drug loadings. The scale bars represent 500 nm.

Intrigued by these interesting findings on PNIPAm homopolymers, a random copolymer of N-isopropylacrylamide/acrylamide (PNIPAm-PAA, $M_w = 15 \text{ kDa}$, the NIPAm/Am molar ratio is 3.1:1) and a block copolymer of PNIPAm and poly(acrylic acid) (PNIPAm-PAA, M_w of PAA and PNIPAm was 10 and 24 kDa, respectively) were used to uncover the structural effect of host polymers, with IND as the model guest molecule. At the IND/PNIPAm-PAA feeding ratio of 0.1:1 (5.8% IND in resulting assemblies), particles of 74 nm were obtained (Fig. 5a (i)), while 476 and 594 nm-sized spherical core-shell nanoassemblies formed at IND/PNIPAm-PAA feeding of 0.2:1 (12.1% IND) and 0.4:1 (26.4% IND) (Fig. 5a (ii-iii) and S10b). Like PNIPAm, additional increment in the IND/PNIPAm-PAA ratio to 0.6:1 (36.2% IND), 0.8:1 (41.4% IND), or 1:1 (49.5% IND) afforded microscaled vesicles (Fig. 5a (iv-vi) and S10b). By contrast, at 2:1 (61.8% IND) and 3:1 (75.5% IND), partly filled vesicles and solid nanospheres were assembled, respectively (Fig. 5a (vii-viii)). As a result, structures varying from micelle-like core-shell nanoassemblies, vesicles, to solid spherical assemblies could also be readily fabricated by one-step assembly of the PNIPAm-PAA random copolymer and IND. Compared with PNIPAm, the vesicular structure of PNIPAm-PAA/IND appeared at a higher IND content, and this should be associated with the more hydrophilic nature of PNIPAm-PAA. Similar to PNIPAm homopolymer, the formation of pseudo amphiphiles with different hydrophilic-hydrophobic balance might be accountable for these diverse structures (Fig. 5a (ix)). Likewise, evolution of multi-structured assemblies was realized for PNIPAm-PAA as shown by both SEM and TEM images (Fig. 5b). At the IND/PNIPAm-PAA ratio of 0.3:1 (19.5% IND in final particles), core-shell spheres could be obtained (Fig. 5b (i)), while vesicles formed at 0.5:1, 1:1, 1.5:1, and 2:1 (the actual IND content was 32.4%, 49.8%, 58.5%, and 64.7%, respectively; Fig. 5b (ii-v)). Further, the size of vesicles was evidently increased with IND (Fig. S10c). At 2:1 of IND/PNIPAm-PAA (64.7% IND in assemblies), we could observe some solid nanospheres, while almost all the formed spheres were solid at 3:1 (74.3% IND, Fig. 5b (vi)).

Collectively, our results indicated that evolution of multiple structures is common for hydrophobic CBC guests mediated assembly of PNIPAm and its copolymers. Nevertheless, the hydrophobic content required for the specific assemblies is strongly dependent on the composition and structure of host polymers. Accordingly, this one-pot assembly strategy may serve as a powerful approach towards multiple superstructures, considering the large number of NIPAm-containing polymers we can easily synthesize and numerous CBCs commercially available.

Co-assembly in the presence of inert hydrophobic molecules

We further interrogated the impact of inert hydrophobic compounds (without carboxyl) on assembly of CBCs and PNIPAm, because it is meaningful for packaging and delivering other carboxyl-deficient hydrophobic therapeutics. Initially, IND was utilized as the model CBC, while paclitaxel (PTX), a highly hydrophobic drug widely used for the treatment of diverse cancers and coronary artery disease, was studied as an inert model compound (Table S2). Co-assembly of PNIPAm (Mw = 10 kDa), IND, and PTX was also performed by the one-pot strategy using DMSO as the common solvent. Whereas dialysis of PTX alone led to crystals (Fig. S11), sphere-shaped and well-dispersed assemblies were generated by PNIPAm/IND/PTX at various weight ratios, as evidently illustrated by SEM and TEM images (Fig. 6a). Compared with the corresponding PNIPAm/IND assemblies, incorporation of PTX dramatically increased the size of resulting microspheres (Fig. S12). The mean size was 1284, 1106, 984 nm for microspheres at PNIPAm/IND/PTX ratios of 1:2:0.5, 1:2:1, and 1:2:2, respectively. TEM examination revealed these assemblies were solid, with a compact interior (Fig. 6a). Likewise, successful co-assembly of PTX with PNIPAm/SUL or PNIPAm/UDCA could be realized, resulting in micrometer-sized, spherical, and solid assemblies (Fig. 6b). We found similar co-assembly performance for another poorly soluble drug of docetaxel (DTX) that is also an effective chemotherapy drug (Table S2 and Fig. 6c). As a result, CBC/PNIPAm can co-assemble with various inert hydrophobic compounds, giving rise to well-shaped spherical assemblies.

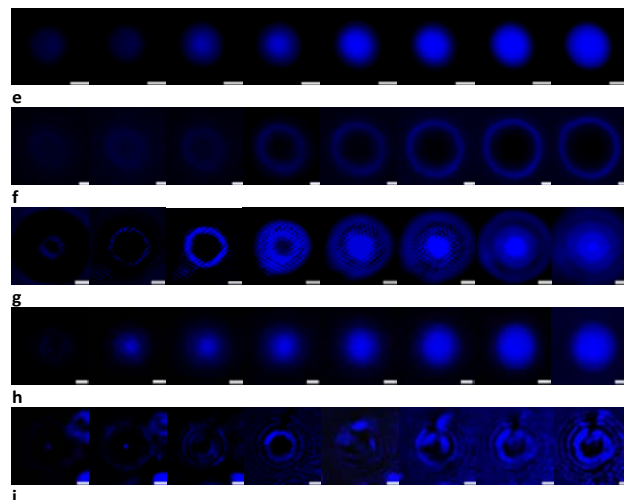
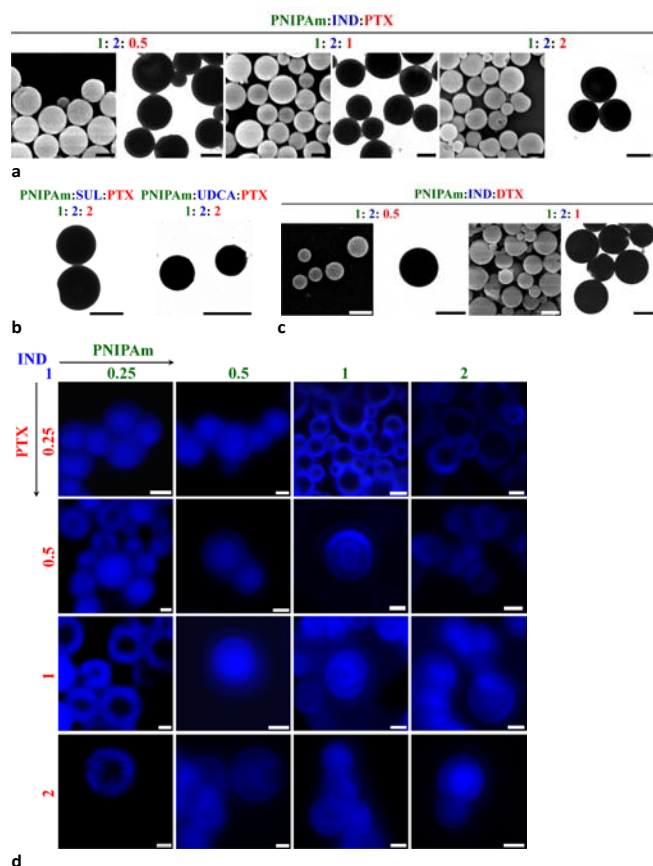


Fig. 6 Co-assembly of CBC/PNIPAm with hydrophobic compounds without carboxyl. **a**, SEM and TEM images of microspheres assembled by PNIPAm/IND with PTX at various weight ratios. **b**, TEM images showing PTX-containing assemblies formed by PNIPAm/SUL or PNIPAm/UDCA. **c**, SEM and TEM micrographs of PNIPAm/IND assemblies with various contents of DTX. **d**, CLSM images with focus plane across the center of different structures formed by PNIPAm/IND/PTX. **e-i**, CLSM images and schematic illustration showing optical sections of microspheres with various structures. For all SEM and TEM images, the scale bar is 1 μm , while it is 500 nm for CLSM images.

Taking advantage of intrinsic fluorescence of IND, we characterized the composite assemblies containing inert compounds by fluorescence microscopy. While PNIPAm/IND/PTX assemblies at various formulations were solid spheres under TEM observation, examination by CLSM revealed distinctly different structures. Keeping the normalized IND content at 1, the relative content of both PNIPAm and PTX was varied from 0.25, 0.5, 1, and 2 (Fig. 6d). With 0.25 of PNIPAm, both solid spheres and vesicles could be observed at PTX contents of 0.25 and 0.5, while increasing PTX to 1 and 2 led to preponderant vesicular structure. Sequential images along z-axis confirmed both solid spherical and vesicular structure (Fig. 6e-f). At 0.5 of PNIPAm and 0.25 or 0.5 of PTX, we observed the Saturn-like structure, i.e. a solid sphere surrounding by a ring. Interestingly, onion-like structure was found at PNIPAm/IND/PTX ratio of 0.5:1:1 and 0.5:1:2, which was further examined by optical sectioning images. The gradually enlarged rings and increased ring numbers corroborated the onion-like, multilayered structure (Fig. 6g). At the PNIPAm content of 1, both fluorescently solid and hollow multilayered microspheres were formed at higher PTX contents of 0.5, 1, and 2 (Fig. 6d and 6h-i), while pure vesicles were reached at PTX of 0.25. Of note, microspheres at PNIPAm/IND/PTX of 1:1:1 had more layers as compared to other formulations, and even 6-layered microspheres could be observed (Fig. 6i and Fig. S13a). Similarly, vesicular and multilayered structures were assembled at PNIPAm of 2, with PTX varying from 0.25 to 2. It should be emphasized that pure PNIPAm/IND microspheres formed at high IND contents did not show any multilayer structure (Fig. S13b-c).

According to these results, presence of PTX is prerequisite for assembly of different structures, and the multilayered

structures require high contents of both PNIPAm and PTX. The formation of these higher-order structures implied the step-by-step or alternative deposition of hydrophobic components during co-assembly. Among three components, inert PTX is the most hydrophobic one. Initially a nucleus might be formed by precipitation of either PTX or PTX/IND mixture, which is followed by deposition of another layer containing IND or PTX, respectively. In both cases, PNIPAm might function as an adhesive component, binding the IND rich layer to the PTX-enriched layer. Moreover, an IND-rich layer occupies the outer surface, as negative zeta-potential values were measured for these assemblies (Fig. S14). Whereas onion-like and multilayered microspheres could be achieved by different methods such as self assembly of amphiphiles^{49,50}, our results denote the first realization of these hierarchical structures by guest molecules mediated assembly of a homopolymer. However, in-depth studies are necessary to address mechanisms underlying the formation of these multilayer structures.

Conclusions

In summary, we showed herein the formation of assemblies with diverse morphologies over multiple length scales, simply by a one-pot strategy of guest molecules-mediated assembly of structurally simple host polymers. The temperature-responsive feature of PNIPAm and its copolymers may afford these superstructures more intriguing attributes such as manipulation on size and shape as well as controlled loading and release of cargo molecules by heat treatment. These assembled nano- and micro-platforms are particularly promising for oral drug delivery. Moreover, this study provides new insights into the design of effective carrier materials for various small-molecular therapeutics.

Experimental

Materials

Azodiisobutyronitrile (AIBN), acrylamide (Am), N-isopropylacrylamide (NIPAm), N-propylacrylamide (NPAm), N,N-dimethylacrylamide (DMAm), N-ethylacrylamide (NEAm), N-methylacrylamide (NMAm), N-hydroxyethyl acrylamide (NHEAm), N-*tert*-butylacrylamide (NTBAm), Nile red, fluorescein O-acrylate, N-acryloxysuccinimide (NASI), *n*-butylamine (BA), *n*-hexylamine (HA), indomethacin (IND), sulindac (SUL), 1-methyl-3-indoleacetic acid (MIAA), flufenamic acid (FLA), (*p*-acetamidophenyl)acetic acid (APA), flurbiprofen (FLUR), ketoprofen (KET), pipemidic acid (PIP), methotrexate (MET), 4-phenylbutyric acid (PBA), retinoic acid (RA), gemfibrozil (GEM), fluvastatin (FLS), pravastatin (PRAS), atorvastatin (ATS), cholic acid (CA), chenodeoxycholic acid (CDCA), hyodeoxycholic acid (HDCA), ursodeoxycholic acid (UDCA), lithocholic acid (LCA), deoxycholic acid (DOCA), and glycodeoxycholic acid (GDCA) were obtained from Sigma-Aldrich (USA). Poly(N-isopropylacrylamide) (PNIPAm) (with Mw of 10, 32, 125, 231, 560, 900, and 1400 kDa), isotactic PNIPAm (isoPNIPAm; iso content > 95%, Mw = 13 kDa), and poly(N-

isopropylacrylamide)-*b*-poly(acrylic acid) (PNIPAm-PAA, the Mw of PNIPAm and PAA was 24 and 10 kDa, respectively) were purchased from Polymer Source (Canada), while polyacrylamide (PAm, Mw = 10 kDa) and PNIPAm with average Mw of 2, 5, and 7 kDa were obtained from Sigma-Aldrich (USA). Poly(lactide-co-glycolide) (50:50) (PLGA) with intrinsic viscosity of 0.50-0.65 was purchased from Polysciences, Inc (USA). Eudragit® S 100 (S100) was kindly supplied by Evonik Industries (Germany). Poly(vinyl alcohol) (PVA) (88 mol% hydrolyzed, Mw = 25 kDa) was obtained from Acro Organics. Paclitaxel (PTX) and docetaxel (DTX) were supplied by Xi'an Xuan Biological Technology Co., Ltd (Xi'an, China). All the other reagents are commercially available and used as received.

Synthesis of polymers

Poly(N-methylacrylamide) (PNMAm), poly(N-ethylacrylamide) (PNEAm), poly(N-propylacrylamide) (PNPAm), poly(N-hydroxyethyl acrylamide) (PNHEAm), poly(N,N-dimethylacrylamide) (PDMAm), and poly(N-*tert*-butylacrylamide) (PNTBAm) were synthesized by free radical polymerization in anhydrous methanol using AIBN as an initiator. The molar ratio of monomer/AIBN was 50:1 in all cases. Polymers were collected by precipitation from diethyl ether, purified by dialysis against deionized water, and then lyophilized to afford white powders. The similar procedures were employed to synthesize fluorescein-labeled PNIPAm by copolymerization of NIPAm with fluorescein O-acrylate. The molar ratio of NIPAm to AIBN was 50:1, while that of NIPAm to fluorescein O-acrylate was 100:1. The copolymer of NIPAm and Am (PNIPAm-PAm) was synthesized by the similar method at the NIPAm/Am molar ratio of 3:1. According to the ¹H NMR spectrum, the molar ratio of NIPAm/Am in the synthesized copolymer was 3.1:1.

The previously established procedure was used to synthesize poly(N-butylacrylamide) (PNBAm) and poly(N-hexylacrylamide) (PNHAM).^{51, 52} To this end, a precursor polymer, i.e. poly(N-acryloxysuccinimide) (PNASI) was synthesized by free radical polymerization in benzene using AIBN as an initiator. The molar ratio of NASI to AIBN was 50:1. PNASI was collected by precipitation from hexane and then dried under vacuum. A subsequent aminolysis of PNASI in the presence of excess amount of BA and HA in anhydrous dimethylformamide (DMF) gave rise to PNBAm and PNHAM, respectively.

Preparation of various assemblies

Assemblies based on PAm, PDMAm, and PNIPAm in the presence of VAL, HEX, and HEP were prepared by directly mixing polymer/aliphatic acid pairs at different weight ratios via vortexing. In other cases, a dialysis procedure was performed. Briefly, various CBC/polymer pairs at different feeding ratios were dissolved in a common solvent (such as DMSO). The obtained solution was dialyzed against deionized water. Unless otherwise stated, the polymer concentration was maintained at 10 mg/mL, and experiments were performed at

25°C. The outer aqueous solution was exchanged every 2 h. After 24 h of dialysis, samples were collected for analysis without further treatment. PNIPAm with Mw of 10 kDa was used with the exception of the study on Mw effect. The drug content of IND and SUL in the lyophilized samples was quantified by UV at 310 nm, while PTX were determined by high-performance liquid chromatography (HPLC).

Calculation of various parameters by group contribution methods

The solubility parameters (δ) of IND and structural units of various polymers were calculated by the method reported by Fedors.⁵³

$$\delta = \left(\frac{\Delta E_v}{V} \right)^{1/2}$$

$$\Delta E_v = \sum_i \Delta e_i$$

$$V = \sum_i \Delta v_i$$

Where ΔE_v is the energy of vaporization at a given temperature and V is the corresponding molar volume, Δe_i and Δv_i are the additive atomic and group contribution for the energy of vaporization and molar volume, respectively.

Both cohesive energy (CE) and cohesive energy density (CED) of various compounds were calculated by the group contribution strategy previously described by Van Krevelen.⁴¹ Also, the partial solubility parameters of δ_d , δ_p , and δ_h , corresponding to contributions from *van der Waals* dispersion forces, dipole-dipole interactions, and H-bonding respectively, were calculated by the method developed by Van Krevelen.⁴¹

$$\delta_d = \frac{\sum F_{di}}{V}$$

$$\delta_p = \frac{\sqrt{\sum F_{pi}^2}}{V}$$

$$\delta_h = \frac{\sum E_{hi}}{V}$$

$$\delta_a = (\delta_p^2 + \delta_h^2)^{1/2}$$

Where F_{di} , F_{pi} , and E_{hi} are the specific functional group contributions of dispersion forces (F_{di}), polar forces (F_{pi}), and H-bonding (E_{hi}). The molar volume (V) of various compounds was obtained by the Fedors' method as described above.⁵³ The polar solubility parameter (δ_a) is the sum of contributions from polar forces and H-bonding.

Molecular modeling

Interactions between typical polymers (PAm, PDMAm, and PNIPAm) and IND were theoretically assessed by molecular modeling (including molecular docking and molecular dynamic). Briefly, the repeat units of polymers including PAm, PDMAm, and PNIPAm were built in three-dimensional (3D) coordinates using the MOE's (Molecular Operating Environment software package, Chemical Computing Group, Canada) builder tool. The polymer chain was built by the head-

to-tail connection with 50 structural units, and 5 repeat units were employed to build short-chain polymers to simulate polymer-polymer interactions in the docking process. The 3D structures of IND, polymers, short-chain polymers, and water molecules were preoptimized before running simulations using the all atom MMFF94x force field with no constraints. Then, IND and water molecules preoptimized were docked into the minimized, hydrated polymer structures using the AutoDock 4.2 software package to estimate the binding energy and intermolecular energies.^{54, 55} IND was docked into the minimized IND molecule to estimate IND-IND interactions. To find the effect of PNIPAm conformation on IND-PNIPAm interactions, the IND/PNIPAm complex with the lowest energy, obtained from docking, was employed to perform molecular dynamic (MD) simulations in water environment using MOE software. Also, a multiple MD simulation containing ten IND molecules was performed to simulate the assembly process of IND/PNIPAm near the actual drug loading. Subsequently, the conformation of PNIPAm obtained from MD stimulations was used in docking studies to predict changes in intermolecular interactions and putative binding sites between PNIPAm and IND.

Measurements

Gel permeation chromatography (GPC) was carried out using a Waters model 1515, equipped with a Waters 2414 refractive index detector. For polymers soluble in THF, THF was used as the mobile phase at a flow rate of 1.0 mL/min, and Mw calibration was performed with polystyrene standards. As for polymers only soluble in water, deionized water containing 0.1% NaN₃ was used as the mobile phase at a flow rate of 1.0 mL min⁻¹, and polyethylene glycols were utilized as standards. ¹H NMR spectra were recorded on a Varian INOVA-400 spectrometer operating at 400 MHz. Fourier transform infrared (FT-IR) spectra were acquired on a Perkin-Elmer FT-IR spectrometer (100S). Particle size and ζ -potential measurements were conducted on a Malvern Zetasizer Nano ZS instrument at 25°C. Transmission electron microscopy (TEM) observation was carried out on a TECNAI-10 microscope (Philips, Netherlands) operating at an acceleration voltage of 80 kV. Formvar coated copper grids were used. Specimens were prepared by dipping the grid into aqueous solution of various samples, and extra solution was blotted with filter paper. After water was evaporated at room temperature, samples were observed directly without any staining. Scanning electron microscopy (SEM) images were taken on a field emission scanning electron microscope (XL30FEG, Phillips). Samples were prepared by coating aqueous solutions of various particles onto freshly cleaved mica, and water was evaporated at room temperature under normal pressure. Confocal laser scanning microscopy (CLSM) observation was performed by a fluorescence microscope (Leica, Heidelberg, Germany). Isothermal titration calorimetry (ITC) experiments were performed using an iTC200 microcalorimeter (MicroCal Inc., GE Healthcare, USA) at 25°C. Specifically, the reference cell was filled with distilled water. An initial 0.4 μ L injection was

discarded from each data set in order to remove the effect of titrant diffusion across the syringe tip during the equilibration process. After the first injection of 0.4 μL of polymer aqueous solution (1 mM) into aqueous solution of CBC (20 μM), 19 times of injection of 2 μL of polymer solution were performed. A background titration was conducted using an identical titrant with deionized water placed in the sample cell, and the result was subtracted from each experimental titration to account for the heat of dilution. The titrant was injected at 2 min intervals to ensure that the titration peak returned to the baseline before the next injection. Each injection lasted for 4 s. To guarantee homogeneous mixing in the cell, the stirring speed was kept at 1000 rpm. Results of titration curves were analyzed using the Origin software supplied by Microcal.

Acknowledgements

This study was financially supported by the National Natural Science Foundation of China (Nos. 81271695 & 81471774) and the Research Foundation of Third Military Medical University (2014XJY04), and also Supported by "Program for New Century Excellent Talents in University (NCET)" of the Ministry of Education.

Notes and references

^a Department of Pharmaceutics, College of Pharmacy, Third Military Medical University, Chongqing 400038, China. E-mail: jxzhang1980@gmail.com; jxzhang@tmmu.edu.cn.

^b Institute of Materia Medica, College of Pharmacy, Third Military Medical University, Chongqing 400038, China. E-mail: lps008@aliyun.com.

^c Department of Pharmacy, Hospital 309 of PLA, Beijing 100091, China.

[†] These authors contributed equally to this work.

†Electronic Supplementary Information (ESI) available: Tables S1-4 and Fig. S1-14. See DOI: 10.1039/b000000x/

- G. M. Whitesides and B. Grzybowski, *Science*, 2002, **295**, 2418-2421.
- O. Ikkala and G. Brinke, *Science*, 2002, **195**, 2407-2409.
- S. Mann, *Nat. Mater.*, 2009, **8**, 781-792.
- A. V. Pinheiro, D. Han, W. M. Shih and H. Yan, *Nat. Nanotechnol.*, 2011, **6**, 763-772.
- X. Ji, Y. Yao, J. Li, X. Yan and F. Huang, *J. Am. Chem. Soc.*, 2013, **135**, 74-77.
- M. Zhang, D. Xu, X. Yan, J. Chen, S. Dong, B. Zheng and F. Huang, *Angew. Chem. Int. Ed.*, 2012, **51**, 7011-7015.
- X. Yan, D. Xu, X. Chi, J. Chen, S. Dong, X. Ding, Y. Yu and F. Huang, *Adv. Mater.*, 2012, **24**, 362-369.
- J. X. Zhang, X. D. Li and X. H. Li, *Prog. Polym. Sci.*, 2012, **37**, 1130-1176.
- H. Sai, K. W. Tan, K. Hur, E. Asenath-Smith, R. Hovden, Y. Jiang, M. Riccio, D. A. Muller, V. Elser, L. A. Estroff, S. M. Gruner and U. Wiesner, *Science*, 2013, **341**, 530-534.
- Z. H. Nie and E. Kumacheva, *Nat. Mater.*, 2008, **7**, 277-290.
- I. Bitá, J. K. Yang, Y. S. Jung, C. A. Ross, E. L. Thomas and K. K. Berggren, *Science*, 2008, **321**, 939-943.
- R. Ruiz, H. Kang, F. A. Detcheverry, E. Dobisz, D. S. Kercher, T. R. Albrecht, J. J. de Pablo and P. F. Nealey, *Science*, 2008, **321**, 936-939.
- M. Sarikaya, C. Tamerler, A. K. Y. Jen, K. Schulten and F. Baneyx, *Nat. Mater.*, 2003, **2**, 577-585.
- Y. G. Wang, K. J. Zhou, G. Huang, C. Hensley, X. N. Huang, X. P. Ma, T. Zhao, B. D. Sumer, R. J. DeBerardinis and J. M. Gao, *Nat. Mater.*, 2014, **13**, 204-212.
- X. H. Liu, X. B. Jin and P. X. Ma, *Nat. Mater.*, 2011, **10**, 398-406.
- J. X. Zhang, S. H. Li and X. H. Li, *Recent Pat. Nanotechnol.*, 2009, **3**, 225-231.
- J. X. Zhang and P. X. Ma, *Adv. Drug Deliv. Rev.*, 2013, **65**, 1215-1233.
- L. Tayebi, Y. C. Ma, D. Vashae, G. Chen, S. K. Sinha and A. N. Parikh, *Nat. Mater.*, 2012, **11**, 1074-1080.
- S. Q. Zhou, C. Burger, B. Chu, M. Sawamura, N. Nagahama, M. Toganoh, U. E. Hackler, H. Isobe and E. Nakamura, *Science*, 2001, **291**, 1944-1947.
- S. G. Zhang, *Nat. Biotechnol.*, 2003, **21**, 1171-1178.
- M. R. Diehl, K. C. Zhang, H. J. Lee and D. A. Tirrell, *Science*, 2006, **311**, 1468-1471.
- F. A. Aldaye, A. L. Palmer and H. F. Sleiman, *Science*, 2008, **321**, 1795-1799.
- J. B. Lee, J. Hong, D. K. Bonner, Z. Poon and P. T. Hammond, *Nat. Mater.*, 2012, **11**, 316-322.
- G. Yu, X. Zhou, Z. Zhang, C. Han, Z. Mao, C. Gao and F. Huang, *J. Am. Chem. Soc.*, 2012, **134**, 19489-19497.
- G. Yu, M. Xue, Z. Zhang, J. Li, C. Han and F. Huang, *J. Am. Chem. Soc.*, 2012, **134**, 13248-13251.
- J. X. Zhang and P. X. Ma, *Nano Today*, 2010, **5**, 337-350.
- L. F. Zhang and A. Eisenberg, *Science*, 1995, **268**, 1728-1731.
- S. Jain and F. S. Bates, *Science*, 2003, **300**, 460-464.
- Z. B. Li, E. Kesselman, Y. Talmon, M. A. Hillmyer and T. P. Lodge, *Science*, 2004, **306**, 98-101.
- X. S. Wang, G. Guerin, H. Wang, Y. Wang, I. Manners and M. A. Winnik, *Science*, 2007, **317**, 644-647.
- D. E. Discher and A. Eisenberg, *Science*, 2002, **297**, 967-973.
- D. J. Pochan, Z. Y. Chen, H. G. Cui, K. Hales, K. Qi and K. L. Wooley, *Science*, 2004, **306**, 94-97.
- H. G. Cui, Z. Chen, S. Zhong, K. L. Wooley and D. J. Pochan, *Science*, 2007, **317**, 647-650.
- M. Schappacher and A. Deffieux, *Science*, 2008, **319**, 1512-1515.
- D. Y. Yan, Y. F. Zhou and J. Hou, *Science*, 2004, **303**, 65-67.
- N. Kamaly, Z. Xiao, P. M. Valencia, A. F. Radovic-Moreno and O. C. Farokhzad, *Chem. Soc. Rev.*, 2012, **41**, 2971-3010.
- Z. L. Cheng, A. A. Zaki, J. Z. Hui, V. R. Muzykantov and A. Tsourkas, *Science*, 2012, **338**, 903-910.
- V. J. Venditto and F. C. Szoka, *Adv. Drug Deliv. Rev.*, 2013, **65**, 80-88.
- G. H. Chen and A. S. Hoffman, *Nature*, 1995, **373**, 49-52.
- B. C. Hancock, P. York and R. C. Rowe, *Int. J. Pharm.*, 1997, **148**, 1-21.
- D. W. van Krevelen, ed., *Cohesive properties and solubility*, 3 edn., Elsevier Science Publisher B.V., Amsterdam, 1990.
- A. F. M. Barton, *Chem. Rev.*, 1974, **75**, 731-753.
- E. B. Bagley, T. P. Nelson and J. M. Scigliano, *J. Paint Technol.*, 1971, **43**, 35-42.
- X. C. Tang, M. J. Pikal and L. S. Taylor, *Pharm. Res.*, 2002, **4**, 484-490.
- H. G. Schild, *Prog. Polym. Sci.*, 1992, **17**, 163-249.
- Y. Y. Ma and A. Eisenberg, *Chem. Soc. Rev.*, 2012, **41**, 5969-5985.
- C. Wu and S. Q. Zhou, *Macromolecules*, 1995, **28**, 5388-5390.
- J. P. Hill, W. Jin, A. Kosaka, T. Fukushima, H. Ichihara, T. Shimomura, K. Ito, T. Hashizume, N. Ishii and T. Aida, *Science*, 2004, **304**, 1481-1483.
- Y. F. Lu, H. Y. Fan, A. Stump, T. L. Ward, T. Rieker and C. J. Brinker, *Nature*, 1999, **398**, 223-226.
- H. W. Shen and A. Eisenberg, *Angew. Chem. Int. Ed.*, 2000, **39**, 3310-3312.
- D. E. Bergbreiter, R. Hughes, J. Besinaiz, C. M. Li and P. L. Osburn, *J. Am. Chem. Soc.*, 2003, **125**, 8244-8249.
- X. Zhou, X. D. Li, T. Mao, J. X. Zhang and X. H. Li, *Soft Matter*, 2011, **7**, 6264-6272.
- R. F. Fedors, *Polym. Eng. Sci.*, 1974, **14**, 147-154.
- G. M. Morris, R. Huey, W. Lindstrom, M. F. Sanner, R. K. Belew, D. S. Goodsell and A. J. Olson, *J. Comput. Chem.*, 2009, **30**, 2785-2791.
- A. D. Costache, L. Sheihet, K. Zaveri, D. D. Knight and J. Kohn, *Mol. Pharmaceutics*, 2009, **6**, 1620-1627.